International Journal of Refractory Metals & Hard Materials 80 (2019) 238–242

Contents lists available at ScienceDirect

International Journal of Refractory Metals & Hard Materials

journal homepage: www.elsevier.com/locate/IJRMHM

Effect of titanium addition on mechanical properties of Mo-Si-B alloys

Won June Choi[a], Seung Yeong Lee[a], Chun Woong Park[a], Jung Hyo Park[b], Jong Min Byun[c,*], Young Do Kim[a,**]

[a] Department of Materials Science and Engineering, Hanyang University, Seoul 04763, Republic of Korea
[b] Agency for Defense Development, Daejeon 34186, Republic of Korea
[c] Department of Materials Science and Engineering, Seoul National University of Science and Technology, Seoul 01811, Republic of Korea

ARTICLE INFO

Keywords:
Mo-Ti-Si-B alloy
Titanium
High energy ball milling
Oxygen gettering
Fracture toughness

ABSTRACT

In this study, we investigated the effect of titanium addition on microstructure and mechanical properties in Mo-Si-B alloys. The Mo-Ti-Si-B alloy (Mo-3.9Ti-3Si-1B, wt%), which has α-Mo, Mo_3Si, Mo_5SiB_2 and TiO_2 phases, was fabricated by a powder metallurgy (PM) method. The starting materials were pulverized by using a high-energy ball milling and the resultant powder was subjected to a reduction process followed by cold isostatic pressing (CIP) compaction and pressureless sintering. In the microstructure, intermetallic compound phases were uniformly distributed in the α-Mo matrix. Some titanium atoms solved into the α-Mo matrix and the others formed a TiO_2 phase caused by reaction with oxygen at the grain boundary. Fracture toughness of the Mo-Ti-Si-B sintered body was recorded as 10.42 $MPa{\cdot}m^{1/2}$, which is lower than that of the Mo-Si-B sintered body without addition of titanium. In the Mo-Ti-Si-B sintered body, the fracture mode is similar to the Mo-Si-B sintered body where intergranular fracture through the Mo grain boundary and transgranular fracture cross the intermetallic compound phase. The decrease of fracture toughness is due to the relatively large TiO_2 at the grain boundary, promoting intergranular fracture.

1. Introduction

The gas turbine, which is one of the typical internal combustion engines, is widely used in various fields such as aerospace and power plants. In gas turbine combustion, burning fossil fuels reach internal temperatures of about 1300 °C [1]. Materials that have high melting points and excellent mechanical properties at elevated temperatures are essential to endure extreme environments and prevent catastrophic failure. Nickel-based superalloys have been utilized for their favorable mechanical properties at high temperature [2]. However, due to the relatively low melting point (T_m: about 1300 °C), the operating temperature of the gas turbine is limited to around 1100 °C [1], thus causing loss of energy efficiency. As a result, materials which have a high melting point and superior mechanical properties at elevated temperatures have been required to substitute for Nickel-based superalloys.

The Mo-Si-B alloys are some of the candidates as next generation high temperature alloys [1,3]. They have a high melting point above 2000 °C and superior mechanical properties at high temperature compared to Nickel-based superalloys. Especially, Mo-Si-B alloys having an α-Mo phase as the matrix and intermetallic compound phases composed of Mo_5SiB_2 and Mo_3Si as the dispersion have been spotlighted [4–8]. The former phase has relatively ductile properties, and the latter phases have excellent mechanical properties with good oxidation resistance at high temperature [9–12]. However, these materials have struggled in applications due to several other problems such as high density and insufficient fracture toughness at room temperature.

Therefore, we investigate Mo-Si-B alloys with the addition of titanium, which is expected to lower the theoretical density, and the effect on microstructure and mechanical property. High energy ball milling was conducted to pulverize the raw materials powder. This ball-milled powder was heat-treated to reduce the MoO_3 phase to the Mo phase which has a 100- to 200-nm particle size range, favorable for sintering at relatively low temperature. The compaction was conducted by using cold isostatic pressing (CIP) and the green body was sintered at 1400 °C for 5 h in a H_2 atmosphere. The microstructure and mechanical property of the resultant alloy were studied.

* Correspondence to: J. M. Byun, Department of Materials Science and Engineering, Seoul National University of Science and Technology, 232 Gongneung-ro, Nowon-gu, Seoul 01811, Republic of Korea.
** Correspondence to: Y. D. Kim, Department of Materials Science and Engineering, Hanyang University, 222 Wangsimni-ro, Seongdong-gu, Seoul 04763, Republic of Korea.
E-mail addresses: byun@seoultech.ac.kr (J.M. Byun), ydkim1@hanyang.ac.kr (Y.D. Kim).

https://doi.org/10.1016/j.ijrmhm.2019.01.019
Received 7 November 2018; Received in revised form 16 January 2019; Accepted 17 January 2019
Available online 17 January 2019

Table 1
Nominal composition of Mo-Si-B [21] and Mo-Ti-Si-B alloys in weight percent.

Specimen	Mo	Ti	Si	B
Mo-Si-B [21]	Bal.	–	3	1
Mo-Ti-Si-B	Bal.	3.9	3	1

2. Experimental procedure

2.1. Fabrication of Mo-Si-B intermetallic compound powder

The Mo-Si-B intermetallic compound powder which consists of Mo_5SiB_2 and Mo_3Si phases were fabricated through the ball milling process followed by a reduction and reaction process. MoO_3 (Kojundo Chemical, Japan, 99.9%), Si_3N_4 (Accumet Materials Co., US, 99%), and BN (Kojundo Chemical, Japan, 99.9%) were used as precursors of Mo, Si and B elements during the milling process, respectively. This ball-milled powder was heat-treated by using an electric furnace in a H_2 atmosphere to produce Mo-Si-B intermetallic compound powder with a nominal composition of Mo-16.6Si-16.7B (at.%). The specific procedure and conditions were described in our previous research [13,14].

2.2. Pulverization of MoO_3, TiH_2 and as-synthesized intermetallic compound powder using high-energy ball milling

A pure MoO_3, TiH_2 (Kojundo Chemical, Japan, 98%) and as-synthesized intermetallic compound powder were used to fabricate the Mo-Ti-Si-B alloys. The composition of this alloy is stated in Table 1. The TiH_2 as a precursor of titanium was added to lower the theoretical density of Mo-Si-B alloys below 9.2 g/cm^3. The high-energy ball milling is conducted by using planetary milling (PM 400, Retsch) for up to 30 h in an Ar atmosphere with 15:1 ball to powder ratio (BPR) and 300 rpm milling speed.

2.3. Reduction of as-milled powder and the sintering process

The high energy ball-milled powder was heat-treated to reduce the MoO_3 phase in as-milled powder to the Mo phase. The reduction mechanism from MoO_3 to the Mo phase is well-known and described in previous research [15,16]. Reduction was conducted by using an electric furnace in a H_2 atmosphere at 10 °C/min to 600 °C and 0.7 ℓ/min H_2 flow. This reduced powder was carefully moved into a glove box which was maintained in a high purity Ar atmosphere to prevent oxidation. The powder was compacted by using CIP with 190 MPa pressure for 5 min. Sintering was conducted in a H_2 atmosphere at a flow rate of 0.7 ℓ/min H_2 at 10 °C/min to 600 °C.

2.4. Analysis

X-ray diffraction analysis (XRD, Rigaku, miniFlex600) with Cu K_α radiation (0.1542 nm) generated at 40 kV was performed to identify phases in powder and sintered bodies. Also, using XRD results, crystalline sizes of the high energy ball-milled powder were calculated using the Williamson-Hall method [17]. The porosity of each specimen was measured by using Archimedes' method. The fracture toughness of sintered bodies was measured by a 3-point bending test. The specimens for this test and several test conditions carefully comply with the ASTM E1820-13 standard [18]. The microstructures of sintered bodies and their fracture surfaces resulting from the 3-point bending test were observed using field emission scanning electron microscope (FE-SEM, NOVA NANO SEM 450, FEI).

3. Results and discussion

Fig. 1 shows XRD patterns of the high energy ball-milled powder which was composed of MoO_3, TiH_2 and as-synthesized intermetallic compound phases with different milling time up to 30 h. Samples acquired below 5 h milling time, showed that all peaks of each phase were broadened with increasing milling time. When milling time exceeded 7 h, most of the MoO_3 peaks were broadened and only intermetallic compound phases remained. When the milling time exceeded 15 h, MoO_2 peaks newly appeared and it is assumed that TiH_2 is decomposed during high-energy ball milling [19]. The MoO_3 phase and H_2 gas from TiH_2 decomposition react together forming the MoO_2 phase [20].

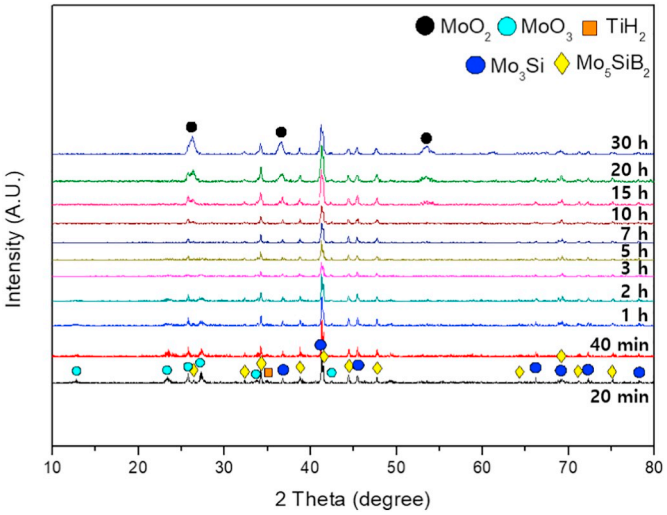

Fig. 1. XRD patterns of high-energy ball milled powder composed of MoO_3, TiH_2 and as-synthesized intermetallic compound phases (Mo_3Si and Mo_5SiB_2) with different milling times.

Fig. 2 presents the crystalline size of the high energy ball milled powder versus milling time. A crystalline size is calculated from XRD results using Williamson-Hall method [17], as shown in Eq. (1):

$$\beta\cos\theta = \frac{\kappa\lambda}{D} + 4\varepsilon\sin\theta \tag{1}$$

where β = full width at half maximum (FWHM), θ = Bragg diffraction angle, κ = Scherrer constant, λ = wavelength of $Cu_{K\alpha}$, D = crystalline size and ε = average internal strain. A peak of intermetallic compound phase is used to calculate crystalline size because other phases are not distinguishable from the noise signal due to peak broadening. The

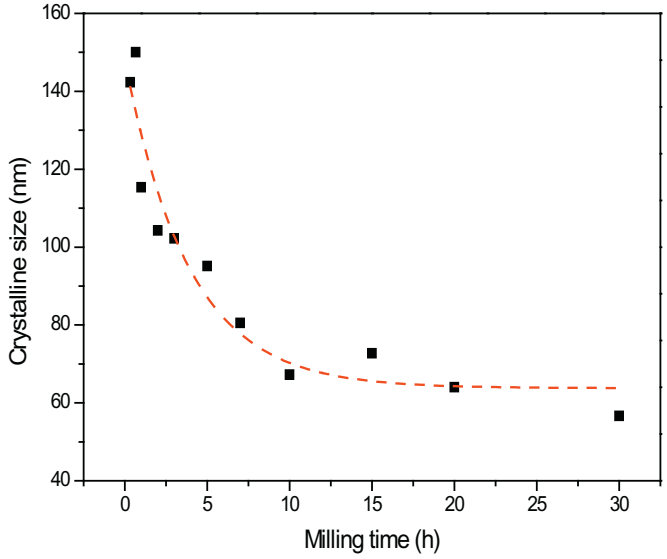

Fig. 2. Crystalline size versus ball milling time, as calculated from XRD analysis by using the Williamson-Hall method.

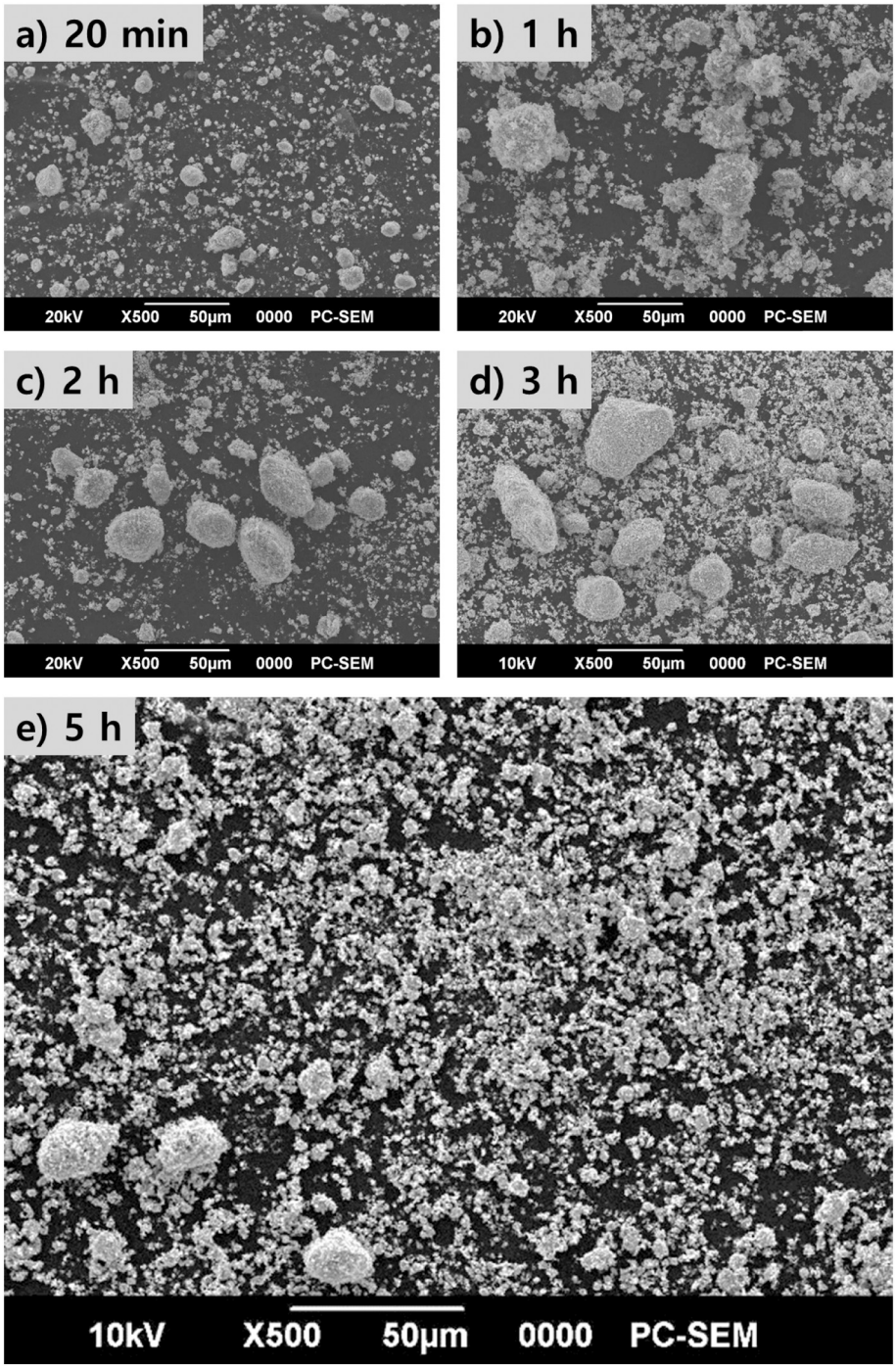

Fig. 3. SEM images of high-energy ball milled powder with different milling times: a) 20 min, b) 1 h, c) 2 h, d) 3 h and e) 5 h.

initial powder without milling has almost 140 nm crystalline size or above. Crystalline size decreased drastically during the initial milling stage and with increasing milling time. Saturation was reached at almost 70 nm crystalline size and more than 10 h milling time. Crystalline size did not change after 10 h milling time.

Fig. 3 shows the SEM images of ball-milled powder with various milling times. In Fig. 3(a), 20-min milled powder had not yet pulverized and powder with different sizes were mixed. In Fig. 3(b)-(d), the amount of powder with submicron sizes gradually increased with increasing milling time, and the agglomeration of submicron powder was observed in SEM images. This powder agglomeration is generally caused by high surface energy of the powder with submicron size. The powder which was ball-milled for 5 h as shown in Fig. 3(e) has uniform particle size with relatively fewer agglomeration of powder. Considering the all of the analysis related to the ball-milled powder, the 5-hour ball-milled powder was chosen to fabricate a Mo-Ti-Si-B sintered body.

The 5-hour ball-milled powder was heat-treated to reduce the MoO_3 phase to the Mo phase with nano-sized powder. The phase transformation was analyzed by using XRD analysis and it is shown in Fig. 4. After the reduction process, the Mo_3Si and Mo_5SiB_2 phases did not react with other phases. The Mo phase which was reduced from the MoO_3 phase newly appeared, showing no evidence of the remaining MoO_3 phase. A small amount of TiO_2 phase was detected through XRD analysis. This phase is probably produced by reaction of the titanium phase and oxygen during the reduction process. This reduced powder was used to fabricate the Mo-Ti-Si-B sintered body.

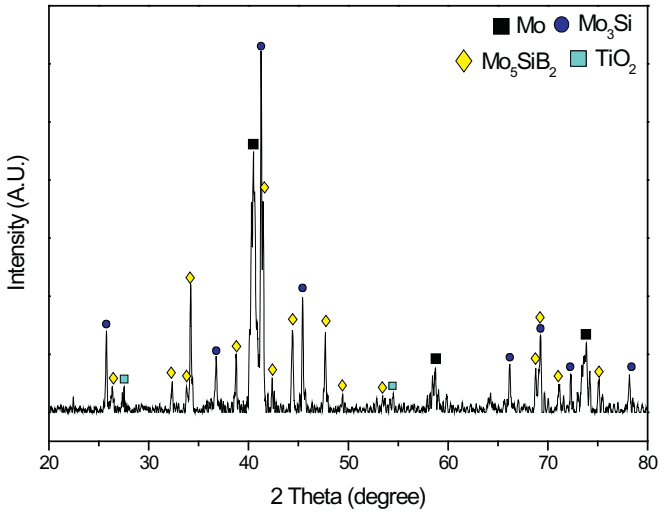

Fig. 4. XRD patterns of reduced powder at 600 °C for 3 h which have Mo, Mo_3Si, Mo_5SiB_2 and small TiO_2 phases.

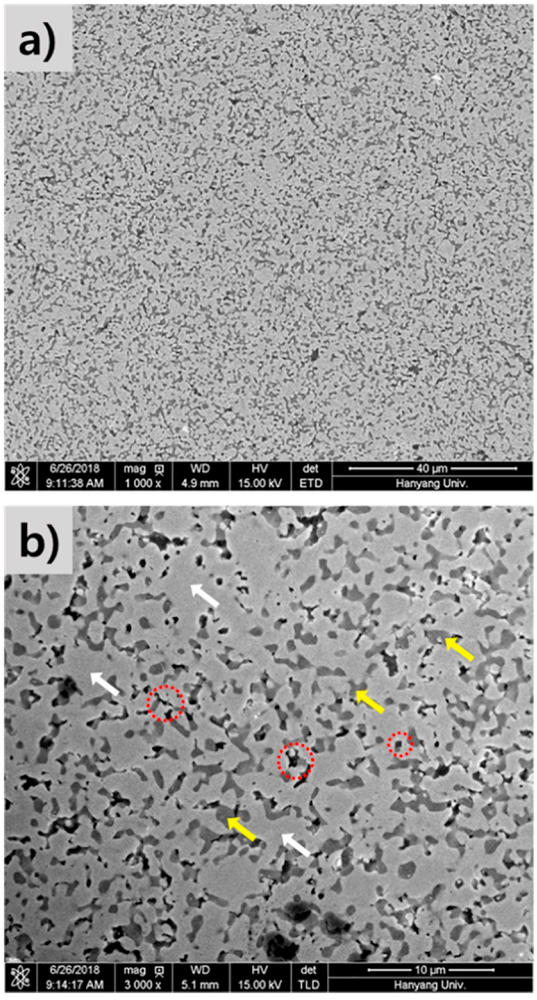

Fig. 5. SEM images of a Mo-Ti-Si-B sintered body which have Mo (white arrow), intermetallic compound (Mo_3Si & Mo_5SiB_2, yellow arrow) and TiO_2 (red dotted circle) phases: a) Intermetallic compound phases (Mo_3Si & Mo_5SiB_2) uniformly distributed in α-Mo matrix, b) High magnification of SEM images of a Mo-Ti-Si-B sintered body. (For interpretation of the references to colour in this figure legend, the reader is referred to the web version of this article.)

The Mo-Ti-Si-B sintered body was fabricated by CIP followed by pressureless sintering. Fig. 5 presents SEM images of the Mo-Ti-Si-B sintered body under varied magnification. The Mo_3Si and Mo_5SiB_2 phases (yellow arrow) were uniformly distributed in the α-Mo matrix (white arrow), as shown in Fig. 5(a). In Fig. 5(b), the TiO_2 phase (red dotted circle), which is formed during the reduction process or sintering process, exist between the α-Mo and intermetallic compound phases. This phase plays a role as an oxygen getter, which is known to trap impurities (O, N, C) and improve mechanical properties by clearing the grain boundary in refractory metals. Fig. 6 presents the XRD analysis of the Mo-Ti-Si-B sintered body which has α-Mo, $MoSi_3$, Mo_5SiB_2 and TiO_2 phases. Compared to the Mo-Si-B sintered body without addition of titanium, the peaks of the Mo phase were slightly shifted to the left side. This is caused by titanium solid solution in the α-Mo matrix due to the difference in atomic radius of each atom. This corresponds to energy dispersive spectrometer (EDS) analysis of the α-Mo matrix. Considering XRD and EDS analysis of the sintered body, some titanium atoms reacted with oxygen and the others solved into the α-Mo matrix.

The fracture toughness of the Mo-Ti-Si-B sintered body was measured by using a 3-point bending test. The Mo-Ti-Si-B sintered body recorded a 10.42 $MPa{\cdot}m^{1/2}$ fracture toughness value, which is as lower than that of the Mo-Si-B sintered body without addition of titanium at

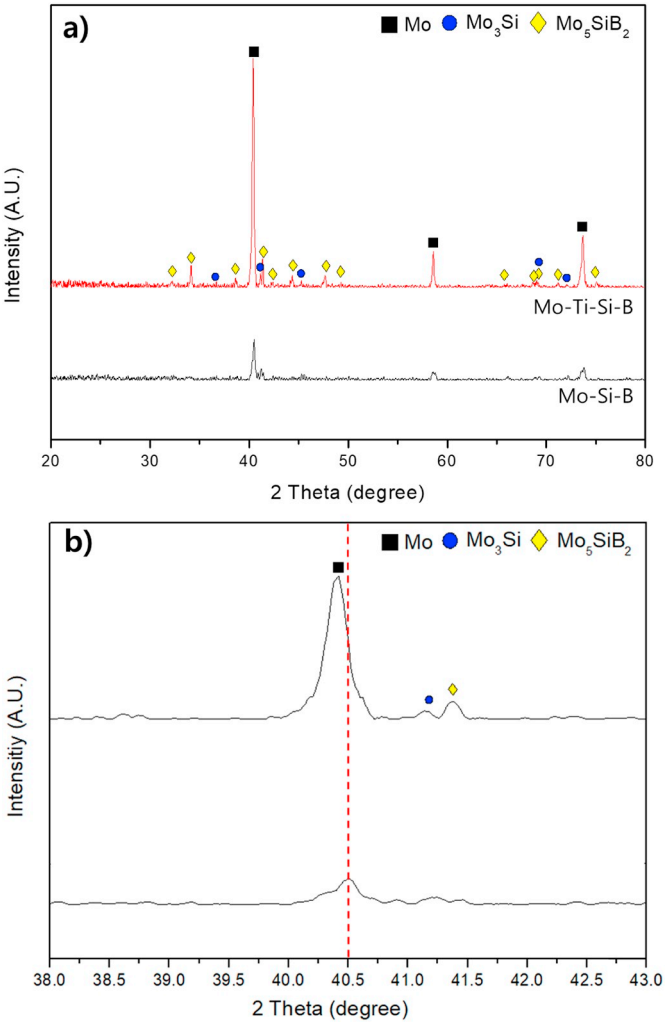

Fig. 6. XRD patterns of a Mo-Ti-Si-B sintered body at 1400 °C for 5 h: a) Comparison of XRD of Mo-Ti-Si-B and Mo-Si-B without addition of titanium, b) Slight shift of the Mo peak in XRD patterns at high magnification of the region of 38–43°.

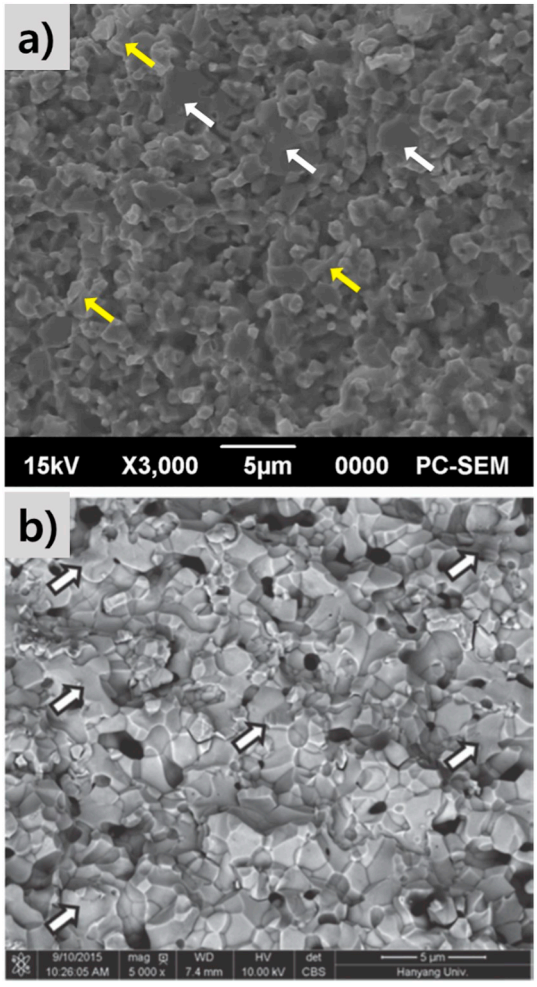

Fig. 7. SEM images of fracture surface after the 3-point bending test: (a) Fracture surface of the Mo-Ti-Si-B sintered body (intergranular fracture: yellow arrow, transgranular fracture: white arrow), (b) Fracture surface of the Mo-Si-B sintered body without addition of titanium [21]. Mixed fracture mode composed of intergranular fracture and transgranular fracture occurred in both sintered bodies. (For interpretation of the references to colour in this figure legend, the reader is referred to the web version of this article.)

12.9 $MPa{\cdot}m^{1/2}$ [21]. Fig. 7 shows the SEM image of the fracture surface of the Mo-Ti-Si-B sintered body and the Mo-Si-B sintered body without addition of titanium after the 3-point bending test [21]. In Fig. 7 (a), intergranular fracture through the Mo grain boundary and transgranular fracture which cross the intermetallic compound phase were observed. This is similar to the results of the Mo-Si-B sintered body without addition of titanium as shown in Fig. 7(b). Dimples were observed at the grain boundary, which are considered as sites TiO_2 particle. Considering Figs. 5 and 7 together, relatively large TiO_2 at the grain boundary might promote intergranular fracture due to stress concentration and grain boundary weakening. It is believed that the decrease in fracture toughness of the Mo-Ti-Si-B sintered body compared to that of Mo-Si-B sintered body are related with respect to microstructure, considering the presence of the TiO_2 phase at grain boundary.

4. Conclusion

In this study, the effect of titanium addition to a Mo-Si-B alloy fabricated by a powder metallurgical method was investigated. MoO_3, TiH_2 and intermetallic compound powder was successfully pulverized by using a high-energy ball milling. This powder was heat-treated in an electric furnace to reduce under a H_2 atmosphere. The Mo-Ti-Si-B sintered body was fabricated by CIP compaction followed by a pressureless sintering process. In the Mo-Ti-Si-B sintered body, intermetallic compound phases were uniformly distributed in the α-Mo matrix. Also, it was found that some titanium atoms reacted with oxygen and the others were solved in the α-Mo matrix. The fracture toughness of the Mo-Ti-Si-B sintered body was measured by a 3-point bending test and the fracture toughness is 10.42 $MPa{\cdot}m^{1/2}$ which is lower than that of the Mo-Si-B sintered body without titanium. The addition of titanium has several advantages such as gettering of impurities and the solid solution effect. However, the relatively large TiO_2 at the grain boundary promotes intergranular fracture caused by stress concentration and grain boundary weakening. In future studies, we will investigate the effects of controlling the amount of titanium addition and size of the oxide particles at the grain boundary and/or grain interior with respect to changes in microstructure and mechanical properties.

Acknowledgement

This work was supported by the Human Resources Program in Energy Technology of the Korea Institute of Energy Technology Evaluation and Planning (KETEP), granted financial resource from the Ministry of Trade, Industry & Energy, Republic of Korea. (No. 20174030201750). This work was also supported by a research fund of the Agency for Defense Development (ADD), Republic of Korea (Project No. UD160078BD).

References

[1] D.M. Dimiduk, J.H. Perepezko, Mo-Si-B alloys: developing a revolutionary turbine-engine material, MRS Bull. 28 (2003) 639–645.
[2] R.C. Reed, The Superalloys: Fundamentals and Applications, 1st ed., Cambridge University Press, Birmingham, 2006.
[3] J.H. Schneibel, C.T. Liu, L. Heatherly, M.J. Kramer, Assessment of processing routes and strength of a 3-phase molybdenum boron silicide (Mo_5Si_3-Mo_5SiB_2-Mo_3Si), Scr. Mater. 38 (1998) 1169–1176.
[4] J.H. Schneibel, M.J. Kramer, Ö. Ünal, R.N. Wright, Processing and mechanical properties of a molybdenum silicide with the composition Mo-12Si-8.5B (at.%), Intermetallics 9 (2001) 25–31.
[5] J.H. Schneibel, M.J. Kramer, D.S. Easton, A Mo–Si–B intermetallic alloy with a continuous α-Mo matrix, Scr. Mater. 46 (2002) 217–221.
[6] T.G. Nieh, J.G. Wang, C.T. Liu, Deformation of a multiphase Mo-9.4Si-13.8B alloy at elevated temperatures, Intermetallics 9 (2001) 73–79.
[7] M. Krüger, S. Franz, H. Saage, M. Heilmaier, J.H. Schneibel, P. Jéhanno, et al., Mechanically alloyed Mo-Si-B alloys with a continuous α-Mo matrix and improved mechanical properties, Intermetallics 16 (2008) 933–941.
[8] O. Hassomeris, G. Schumacher, M. Krüger, M. Heilmaier, J. Banhart, Phase continuity in high temperature Mo–Si–B alloys: A FIB-tomography study, Intermetallics 19 (2011) 470–475.
[9] I. Rosales, J.H. Schneibel, L. Heatherly, J.A. Horton, L. Martinez, B. Campillo, High temperature deformation of A15 Mo_3Si single crystals, Scr. Mater. 48 (2003) 185–190.
[10] K. Ito, K. Ihara, K. Tanaka, M. Fujikura, M. Yamaguchi, Physical and mechanical properties of single crystals of the T2 phase in the Mo-Si-B system, Intermetallics 9 (2001) 591–602.
[11] T. Hayashi, K. Ito, K. Ihara, M. Fujikura, M. Yamaguchi, Creep of single crystalline and polycrystalline T2 phase in the Mo-Si-B system, Intermetallics 12 (2004) 699–704.
[12] F.A. Rioult, S.D. Imhoff, R. Sakidja, J.H. Perepezko, Transient oxidation of Mo–Si–B alloys: Effect of the microstructure size scale, Acta Mater. 57 (2009) 4600–4613.
[13] S.H. Hwang, J.M. Byun, S. Lee, M.J. Suk, S.T. Oh, Y.D. Kim, Fabrication of Mo-Si-B intermetallic powder by mechano-chemical process, J. Alloys Compd. 585 (2014) 418–422.
[14] J.M. Byun, S.H. Hwang, S. Lee, M.J. Suk, S.T. Oh, Y.D. Kim, Microstructure control of Mo–Si–B alloy for formation of continuous α-Mo phase, Int. J. Refract. Met. Hard Mater. 53 (2015) 61–65.
[15] Y.J. Lee, Y.I. Seo, S.H. Kim, D.G. Kim, Y.D. Kim, Optical properties of molybdenum oxide thin films deposited by chemical vapor transport of $MoO_3(OH)_2$, Appl. Phys. A Mater. Sci. Process. 97 (2009) 237–241.
[16] W.V. Schulmeyer, H.M. Ortner, Mechanisms of the hydrogen reduction of molybdenum oxides, Int. J. Refract. Met. Hard Mater. 20 (2002) 261–269.
[17] C. Suryanarayana, M.G. Norton, X-ray diffraction: A practical approach, 1st ed., Springer, New York, 1998.
[18] ASTM: E 1820-13$^{\varepsilon 1}$, Standard Test Method for Measurement of Fracture Toughness, (2014), pp. 1–54.
[19] V. Bhosle, E.G. Baburaj, M. Miranova, K. Salama, Dehydrogenation of TiH_2, Mater. Sci. Eng. A A356 (2003) 190–199.
[20] K.C. Jeon, H.E. Lee, D.M. Yim, S.T. Oh, Effect of heat treatment atmosphere on the microstructure of TiH_2-MoO_3 Powder Mixtures, J. Korean Powder Metall. Inst. 23 (2016) 303–306.
[21] J.M. Byun, S.R. Bang, C.W. Park, M.J. Suk, Y.D. Kim, Structural size effects of intermetallic compounds on the mechanical properties of Mo-Si-B alloy: An experimental investigation, Met. Mater. Int. 22 (2016) 81–86.